Two-Dimensional Finite Element Ablative Thermal Response Analysis of an Arcjet Stagnation Test

John A. Dec[*]
NASA Langley Research Center, Hampton, Virginia, 23681

Bernard Laub[†]
NASA Ames Research Center, Moffett Field, California, 94035

Robert D. Braun[‡]
Georgia Institute of Technology, Atlanta, Georgia, 30332-0150

The finite element ablation and thermal response (FEAtR, hence forth called FEAR) design and analysis program simulates the one, two, or three-dimensional ablation, internal heat conduction, thermal decomposition, and pyrolysis gas flow of thermal protection system materials. As part of a code validation study, two-dimensional axisymmetric results from FEAR are compared to thermal response data obtained from an arc-jet stagnation test in this paper. The results from FEAR are also compared to the two-dimensional axisymmetric computations from the two-dimensional implicit thermal response and ablation program under the same arcjet conditions. The ablating material being used in this arcjet test is phenolic impregnated carbon ablator with an LI-2200 insulator as backup material. The test is performed at the NASA, Ames Research Center Interaction Heating Facility. Spatially distributed computational fluid dynamics solutions for the flow field around the test article are used for the surface boundary conditions.

Nomenclature

2-D	=	two-dimensional
3-D	=	three-dimensional
B_i	=	pre-exponential factor for the ith resin component
c_p	=	solid material specific heat, J/kg-K
C_H	=	Stanton number for heat transfer
CFD	=	computational fluid dynamics
DPLR	=	data parallel line relaxation
E_{ai}	=	activation energy for the ith resin component, J/kg-mole
FEAR	=	finite element ablation and thermal response design and analysis program
FIAT	=	fully implicit ablation and thermal response program
h_g	=	enthalpy of pyrolysis gas, J/kg
$\overline{h}$	=	weighted average solid enthalpy, J/kg
H	=	thermocouple depth, m
i	=	node index, resin component index (A, B ,C)
IHF	=	interaction heating facility
k	=	orthotropic thermal conductivity matrix, W/m-K
$\dot{m}_g''$	=	pyrolysis gas mass flux vector, kg/m^2-s
MSL	=	Mars Science Laboratory

[*]Aerospace Engineer, Structural and Thermal Systems Branch, MS 431, AIAA Member.
[†]Project Manager, Thermal Protection Materials and Systems Branch, MS 234-1, AIAA Associate Fellow
[‡]David and Andrew Lewis Associate Professor of Space Technology, Guggenheim School of Aerospace Engineering, AIAA Fellow

N	=	interpolation, or shape functions
$\hat{n}$	=	unit vector normal to the surface
P	=	pressure, N/m^2
$PICA$	=	phenolic impregnated carbon ablator
$\boldsymbol{q}$	=	net heat flux to the surface
R	=	universal gas constant, J/kg-mole-°K
r	=	thermocouple radial location, m
$\dot{\boldsymbol{S}}$	=	recession rate vector, m/s
T	=	temperature, °C
t	=	time, sec
$TITAN$	=	two-dimensional implicit thermal response and ablation program
TPS	=	thermal protection system
U_e	=	boundary layer edge velocity, m/s
W	=	weighting function
(e)	=	parameter defined over one element
α	=	absoptivity
ΔT	=	temperature difference, °C
Γ	=	resin volume fraction
$\boldsymbol{\kappa_p}$	=	permeability tensor
ρ_A	=	density of first resin component, kg/m^3
ρ_B	=	density of second resin component, kg/m^3
ρ_C	=	density of fiber reinforcement, kg/m^3
ρ_r	=	residual density, kg/m^3
ρ	=	solid material density, instantaneous density, kg/m^3
ρ_o	=	initial density, kg/m^3
ρ_v	=	density of pure virgin material, kg/m^3
ρ_c	=	density of pure char material, kg/m^3
ψ_i	=	density exponent factor
ν	=	kinematic viscosity, m^2/s
ϕ	=	porosity
Ω	=	volume domain
∇	=	gradient operator
$''$	=	denotes flux quantity, 1/m^2

I. Introduction

THERE are two types of thermal protection systems (TPS) in use today, reusable and ablative. Use of reusable TPS, like the space shuttle tiles or a metallic heat sink, are generally limited to low heat flux atmospheric entry, hence forth called entry, trajectories.[1,2] Ablative TPS, on the other hand, can withstand large heat fluxes and heat loads, and are generally used for vehicles which have a high entry velocity, such as ballistic planetary entry missions. In addition to high entry velocity, ablative TPS are also well suited where the target planet has a high atmospheric density, such as Jupiter, since the heating rate is proportional to the density.[3]

Arcjet test facilities, such as the NASA, Ames Research Center Interaction Heating Facility (IHF), provide the primary means to test the performance of TPS materials[4]. Data obtained from these arcjet tests also provide a means with which to validate ablative thermal response computational tools and develop material response models. The finite element ablation and thermal response (FEAtR hence forth called FEAR) design and analysis program was developed to analyze ablative heatshields in multiple dimensions.[5,6] The one-dimensional validation and verification of FEAR was accomplished in Ref. 5. Verification of the three-dimensional (3-D) FEAR results was accomplished in Ref. 4 as well, but the lack of anisotropic material properties, computational fluid dynamics (CFD) solutions, and 3-D arcjet data made full validation problematic, so only partial validation was achieved in Ref 5. Complete validation of the three-dimensional solution is the subject of future work.

The ablating material used in this test was the phenolic impregnated carbon ablator (PICA), which is a low density TPS material developed in the 1990's.[7,8] PICA was successfully flown on the Stardust sample-return capsule as the fore-body heatshield, and is the forebody heatshield for the Mars Science Laboratory entry vehicle. PICA was also one of the final two candidate TPS materials for the Orion Crew Exploration Vehicle heatshield. The Orion TPS Advanced Development Project conducted a large number of arc-jet tests over a wide range of conditions to evaluate the performance of PICA and validate its thermal response model.

FEAR currently supports three and six noded triangle elements as well as four, eight, and nine noded quadrilateral elements. For this study, only four noded quadrilateral elements are compared to the arcjet test data and TITAN. The arcjet data includes measurements of surface temperature, surface recession, and in-depth temperatures. The heat flux, recovery enthalpy, and pressure boundary conditions are provided in the form a two-dimensional (2-D) spatial distribution from the data-parallel line relaxation (DPLR) CFD solution and is decoupled from the thermal response simulation albeit at the expense of losing some fidelity as the shape of the test article changes. In this paper, the 2-D FEAR solution is compared to both PICA arcjet data and solutions from the 2-D implicit thermal-response and ablation (TITAN) program[9,10]. TITAN is a 2-D, implicit finite difference solution scheme for the energy equation and three-component decomposition model with a moving grid. In this paper, the 2-D FEAR solution is compared to both PICA arcjet data and solutions from the TITAN program.

II. Finite Element Ablation and Thermal Response Design and Analysis Program

The governing differential equations which form the basis of the FEAR program describe the ablative thermal response problem and consist of the conservation of mass, momentum, and energy. A detailed derivation of the governing differential equations from first principles is presented in Ref. 5 and summarized in this section. The conservation of mass may be written as

$$\frac{\partial \rho}{\partial t} = -\nabla \dot{m}_g''$$

(1)

The instantaneous density is assumed to be a three-component mixture consisting of two resins and one reinforcing material components and is given by

$$\rho = \Gamma \left(\rho_A + \rho_B \right) + \left(1 - \Gamma \right) \rho_C$$

(2)

The decomposition over time is calculated using an Arrhenius relation[11,12] written as

$$\frac{\partial \rho_i}{\partial t} = -\mathrm{B}_i e^{-E_{a_i}/RT} \rho_{o_i} \left(\frac{\rho_i - \rho_{r_i}}{\rho_{o_i}} \right)^{\psi_i} \quad i = A, B, C$$

(3)

In general, ablative materials are porous materials and the porosity, as well as the permeability, increase as the material decomposes from its virgin state to its charred state. Therefore, Darcy's law is used to calculate the pressure drop due to the flow of pyrolysis gas through the material.

$$\dot{m}_g'' = \frac{-\kappa_p}{\nu \phi} \nabla P$$

(4)

The conservation of energy for the conductive transport of energy through an ablative material that is decomposing in-depth may be written as

$$\rho c_p \frac{\partial T}{\partial t} = k \nabla T + \left(h_g - \bar{h} \right) \frac{\partial \rho}{\partial T} + \dot{m}_g'' \nabla h_g + \dot{S} \rho c_p \nabla T$$

(5)

III. Weak Formulation

The corresponding weak form of the governing system of equations, (1), (4), and (5) may be constructed by first multiplying the residual of the differential equation by an appropriate set of weighting functions W and integrating

by parts over the domain Ω. If the weighting functions W are set equal to the shape functions N which approximate the unknown variables, the result is known as the Bubnov-Galerkin form[13]. The method of weighted residuals requires that the weighted average of the error, or residual, vanish over the solution domain. The weighted residual statement for the conservation of mass and momentum is given in Eqs. (6) and (7), respectively. The weighted residual statement for the conservation of energy is given in Eq. (8).

$$\iiint_{\Omega}\left[\nabla\dot{m}_g''^{(e)}-\frac{\partial\rho}{\partial t}\right]N_i^P d\Omega = 0 \tag{6}$$

$$\iiint_{\Omega}\left[\dot{m}_g''^{(e)}+\frac{\kappa_p}{v\phi}\nabla P^{(e)}\right]N_i^{u,v,w}d\Omega = 0 \tag{7}$$

$$\iiint_{\Omega^{(e)}}\left[k\nabla T^{(e)}+\left(h_g-\bar{h}\right)\frac{\partial\rho^{(e)}}{\partial t}+\dot{m}_g''\nabla h_g^{(e)}+\dot{S}\rho c_p\nabla T^{(e)}-\rho c_p\frac{\partial T^{(e)}}{\partial t}\right]N_i d\Omega = 0 \tag{8}$$

In Eqs. (6) and (7), the shape functions that appear in the mass and momentum equations are different. In this formulation, the shape functions which approximate the pressure must be one order lower than those used to approximate the pyrolysis gas flux components in order to prevent an over constrained system of discrete equations. This formulation makes the pressure discontinuous across element boundaries and thus, pressure is not a primary variable in the weak formulation[14].

Integrating Eqs. (7) and (8) by parts to eliminate the pressure derivative and reduce the derivative on the temperature to first order results in Galerkin's weak form for the conservation of mass, momentum and energy given by Eqs. (9), (10), and (11), respectively.

$$\iiint_{\Omega}\left[\nabla\dot{m}_g''\right]N_i^P dxdydz = \iiint_{\Omega}\frac{\partial\rho}{\partial t}N_i^P \tag{9}$$

$$\iiint_{\Omega}\left(\dot{m}_g''^{(e)}N_i^{u,v,w}\right)dxdydz+\iiint_{\Omega}\frac{\kappa_p}{v\phi}\frac{\partial N_i^{u,v,w}}{\partial x}P^{(e)}dxdydz = \iint_{\Gamma}N_i^{u,v,w}\left(P\cdot\hat{n}\right)d\Gamma+\iint_{\Gamma}N_i^{u,v,w}V_n d\Gamma \tag{10}$$

$$\iiint_{\Omega^{(e)}}\left(k_x\frac{\partial T^{(e)}}{\partial x}\frac{\partial N_i}{\partial x}+k_y\frac{\partial T^{(e)}}{\partial y}\frac{\partial N_i}{\partial y}+k_z\frac{\partial T^{(e)}}{\partial z}\frac{\partial N_i}{\partial z}\right)dxdydz+\iiint_{\Omega^{(e)}}\dot{m}_g''\nabla h_g^{(e)}N_i dxdydz$$
$$+\iiint_{\Omega^{(e)}}\dot{S}\rho c_p\nabla T^{(e)}N_i dxdydz-\iiint_{\Omega^{(e)}}\rho c_p\frac{\partial T^{(e)}}{\partial t}N_i dxdydz+\iint_{\Gamma^{(e)}}\left(\mathbf{q}\cdot\hat{n}\right)N_i d\Gamma = 0 \tag{11}$$

The surface integrals introduced by the integration by parts provide the connection to the surface boundary conditions present on any surface of the element. In the momentum equation, the first surface integral represents surface tractions and the second a specified mass flux at the surface. In the energy equation, the surface integral represents the net conductive flux into the volume, $\Omega^{(e)}$, from any surface bounded by Γ and can be expanded to represent any number of boundary conditions by summation over all surfaces bounded by Γ. Since Eq. (11) is for one element, Γ includes all of the surfaces of the element. For example, in the case of an ablative material, the surface boundary conditions are given by

$$\iint_{\Gamma^{(e)}}\left(\mathbf{q}\cdot\hat{n}\right)N_i d\Gamma = \rho_e U_e C_H\left(H_{sr}-h_{sw}+B_c'h_c+B_g'h_g-B'h_w\right)-q^*+q_{rad_{out}}-\alpha q_{rad_{in}} \tag{12}$$

The governing differential equations for linear elasticity are used to solve for the thermal stress and also to move the mesh while recession is occurring. These governing differential equations and corresponding weak form have been developed and described in detail in several references and are not presented in this paper[13,15].

IV. Arcjet Coupon Geometry and Computational Mesh

One advantage in the FEAR program is that the geometry of the object being analyzed can be created in ProEngineer[®], or any other computer-aided design (CAD) software which has the ability to export the geometry in IGES or STEP file format. Once the geometry is created, the geometry can be imported into MSC PATRAN[®] for meshing, material specification, and boundary condition application. This portability facilitates the design process by allowing designers, and both structural and thermal analysts to have the ability to work with a common model. Data exchange is simplified since the FEAR solution can either be imported back into PATRAN or into Tecplot. The computational geometry being used in this paper was developed in ProEngineer and is based on arcjet test coupons designed and fabricated by NASA, Ames Research Center.[16]

The arcjet coupon is an Iso-Q shape with a 10.16 cm diameter and overall length of 9.78 cm. The coupon is fabricated from two materials, the test material which is PICA, and the backup insulation layer which is LI-2200, a low density silica fiber based ceramic insulator.[17] The PICA cylinder is 4.127 cm diameter in the middle section and 5.08 cm diameter near the edges. The axisymmetric geometry, after being imported into PATRAN, is shown in Fig. 1 with the computational mesh superimposed. The actual arcjet specimen has a 1.78 mm air gap between the PICA and the LI-2200 in the 4.127 cm depth section of the PICA, but the air gap is neglected in this analysis since surface to surface radiation is not currently supported in FEAR. After the geometry is imported into PATRAN, the 3-D solid is broken down into a cross-sectional set of surfaces and only those on one side of the centerline are retained to perform the axisymmetric analysis.

The arcjet coupon geometry was meshed with the meshing routine built within MSC PATRAN[®]. The surfaces were meshed with structured, 4-noded quadrilateral elements. The mesh was biased towards the heated surface and consisted of 1188 nodes and 1119 elements. In the region near the shoulder of the coupon, the mesher produced much smaller elements in order to maintain congruency between the individual geometric surfaces which make up the axisymmetric geometry. Future work will examine different element types such as triangles, wedges, and unstructured quadrilaterals, and also examine the performance of higher order elements.
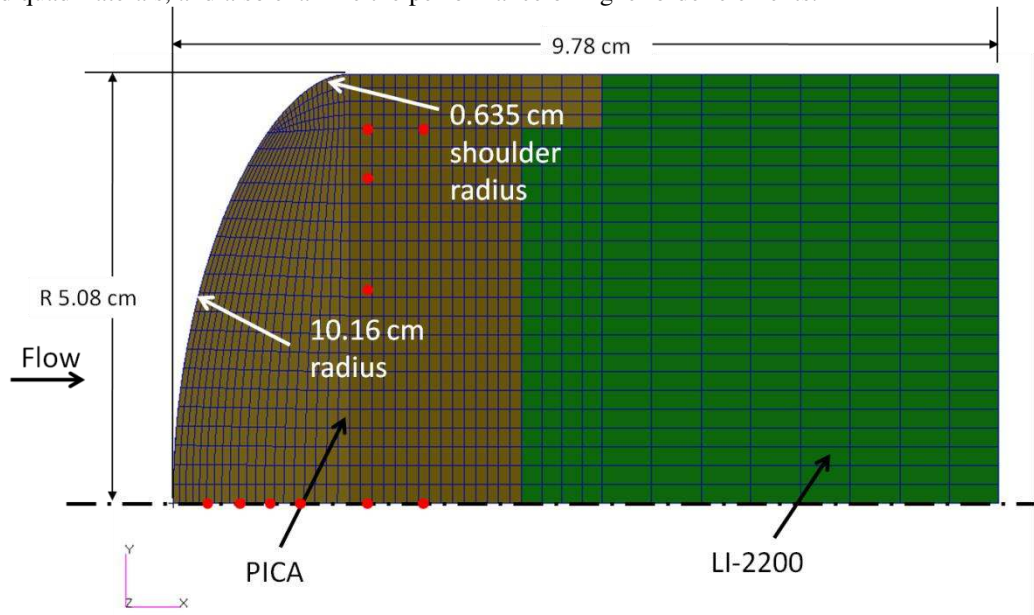

Fig. 1 PICA arcjet coupon geometry and computational mesh.

The arcjet coupon had six thermocouples embedded in-depth in a 2.54 cm plug which was inserted down the centerline. The coupon also had thermocouples at three radial locations at two depths equal to the two deepest thermocouples along the centerline. The thermocouple locations are summarized in Table 1.

Table 1 Thermocouple locations

Designation	Depth, H (cm)	Radial Distance, r (cm)
TC1	0.381	0.0
TC2	0.762	0.0

TC3	1.143	0.0
TC4	1.524	0.0
TC5	2.286	0.0
TC6	3.048	0.0
TC7	2.286	2.54
TC8	2.286	3.81
TC9	2.286	4.45
TC10	3.048	4.45

V. Boundary Conditions

The surface boundary conditions were obtained from a CFD solution of the coupon in the arcjet flow. The centerline enthalpy for this test was 19.3 MJ/kg and the centerline heat flux was 255 W/cm^2. The coupon was exposed to the flow for 40 seconds and allowed to cool. The cool down time for analysis purposes was 600 seconds. The heat flux varied across the surface of the coupon and also wrapped around the shoulder where there was non-trivial sidewall heating calculated. The distributed surface heat flux is shown in Fig. 2 and is applied to the external edges of the PICA and LI-2200.

In addition to the heat flux boundary condition, FEAR requires two supplementary boundary conditions. The first is a no flow boundary condition which is specified on the back edge of the PICA which interfaces with the LI-2200. The no flow boundary condition is required for the solution of the mass and momentum equations. The final required boundary conditions are to specify the zero displacement boundaries. The zero displacement boundaries are required for both the mesh movement scheme and the thermal stress calculation and need not be coincident. The zero displacement boundary condition for the mesh movement scheme encompasses all of the nodes and elements representing the LI-2200 since only the PICA is allowed to recede. The zero displacement boundary for the thermal stress calculation is the bottom edge of the LI-2200. Radiation in or out of any edge, (or surface in 3-D) is not a hard requirement, but is applied to all the external edges of the coupon except for the bottom edge of the LI-2200. The initial temperature is 20°C and the radiation sink temperature is 21.1°C.
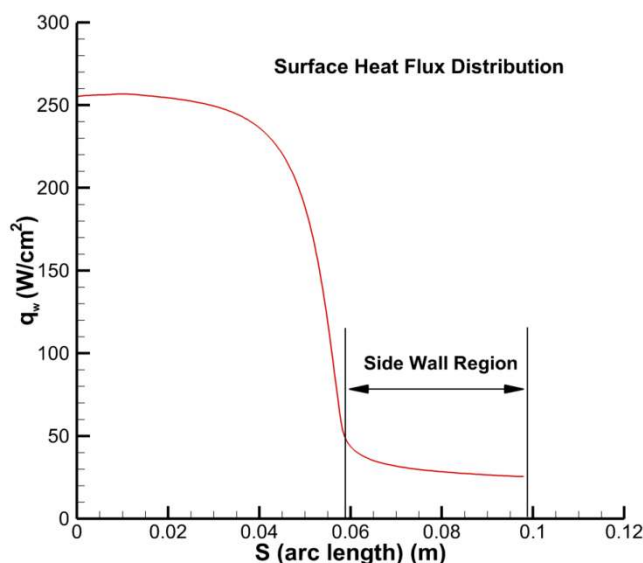

**Fig. 2 CFD predicted surface heat flux distribution.**

VI. Results and Discussion

FEAR was run in 2-D axisymmetric mode for the arcjet conditions and geometry described in Sections IV and V. The temperature distribution at 40 seconds when the arcjet flow is cutoff is shown in Fig. 3. The temperature on the side of the coupon has increased significantly compared to the temperature along the centerline at the same depth, a clear indication that the sidewall heating has a significant affect.
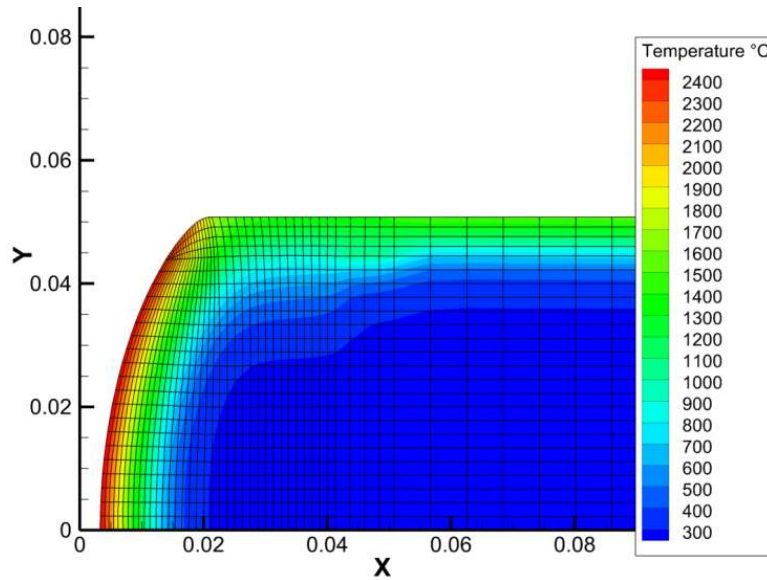
Fig. 3 Temperature distribution at arcjet flow cutoff (40 sec).

The temperature distribution after cooling down for 560 seconds is shown in Fig. 4 and is superimposed on the original outer mold line of the coupon to show the shape change. The coupon maintains the Iso-Q shape, as expected, and the side wall heating is not significant enough to cause recession in the radial direction. Another indication that the side wall heating effects are significant is to examine the density distribution. The final coupon char fraction distribution is shown in Fig. 5. The char profile indicates that the PICA has decomposed significantly near the side of the specimen compared to the same depth along the centerline. The boundary elements between the PICA and LI-2200 share common nodes and as a consequence, the contour plot looks as if there is a severe density gradient in those elements. Computationally, each node has the correct density applied when the element is assembled into the global matrix. Until contact boundary conditions are implemented within FEAR and the boundary elements have independent nodes, this output anomaly for density will have to be tolerated.
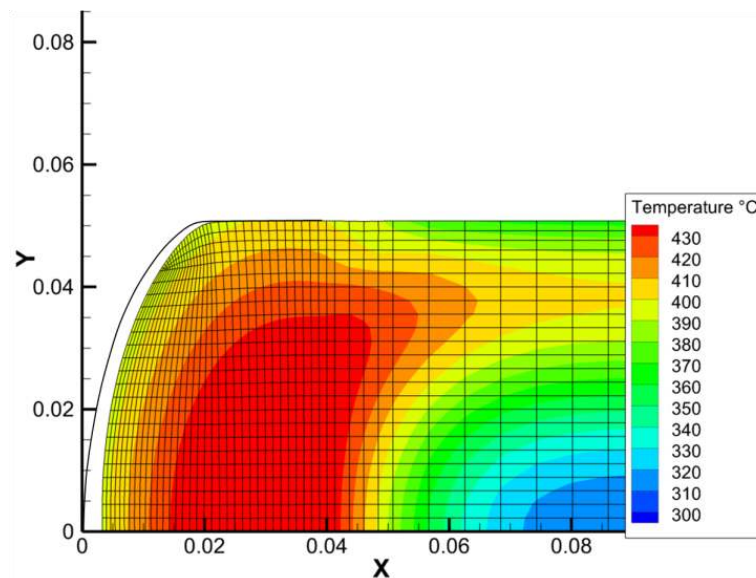

Fig. 4 Temperature distribution after a 560 second cool down.
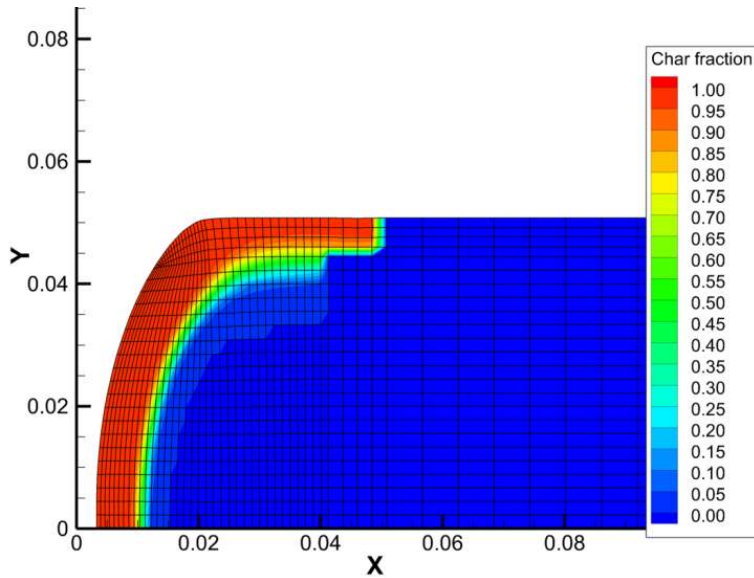
Fig. 5 Final char distribution.

Comparison of the centerline thermocouple arcjet data with the results from both FEAR and TITAN are plotted Fig. 6. There was no pyrometer data available for comparison, but from Fig. 6 both TITAN and FEAR calculate similar surface temperatures. Recession measured on the centerline at the stagnation point was 4.06 mm and the stagnation point recession calculated by FEAR was 3.28 mm, a difference of 0.78 mm. The in-depth centerline temperatures calculated by FEAR compare well with both the TITAN solution and the arcjet data. Comparison of the temperatures along the radial lines at depths of 2.286 cm and 3.048 cm are plotted in Fig. 7 and Fig. 8 respectively. The results from FEAR compares well to both the arcjet data and to the results from TITAN. The radial comparison indicates that the anisotropic material properties and the application of sidewall heating within FEAR are being implemented correctly.
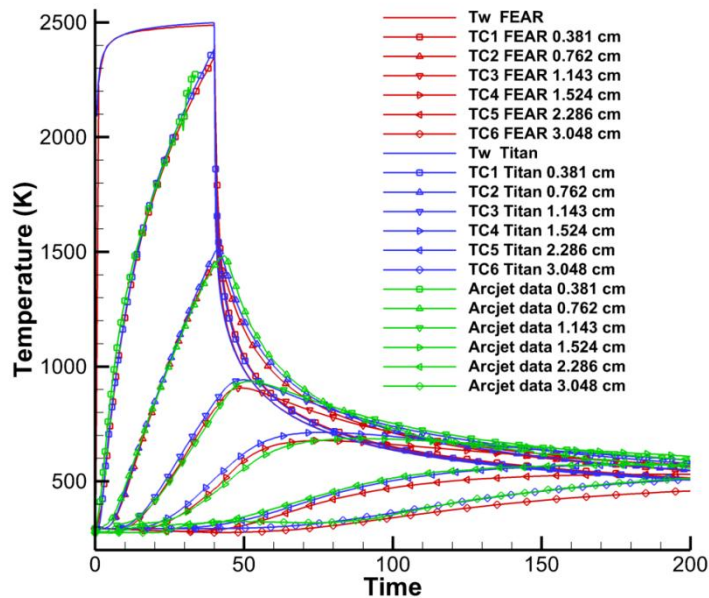
Fig. 6 Centerline thermocouple temperature comparison between FEAR and TITAN

The results from FEAR do not match those of TITAN perfectly. The inputs used by both FEAR and TITAN are referred to as a response model. The differences between FEAR and TITAN arise because of how the response model is developed. The thermal response model used in this study was taken from the Crew Exploration Vehicle

American Institute of Aeronautics and Astronautics

(CEV) Thermal Protection System (TPS) Advanced Development Project (ADP) material property database. This thermal response model was developed with measured material property data and numerous instrumented arcjet tests. The fully implicit ablation and thermal-response (FIAT) program, and the 2-D counterpart TITAN, benefit from the fact that adjustments to the thermal response model are made such that the FIAT solution matches the arcjet data over a wide range of conditions. Typically, the char thermal conductivity is adjusted during this process to account for all the other uncertainties present in the model, but other adjustments, such as altering the pyrolysis gas and virgin material compositions are also made.
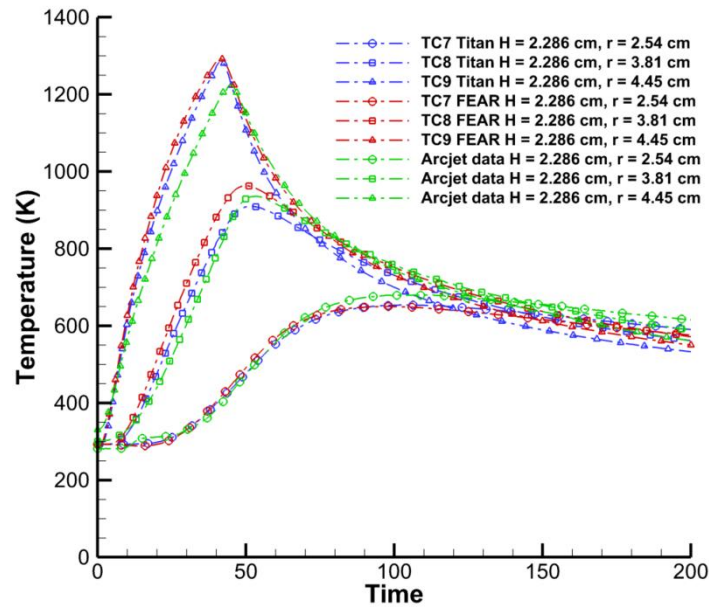

Fig. 7 Temperature comparison between FEAR and TITAN along a radial line at a depth of 2.286 cm.
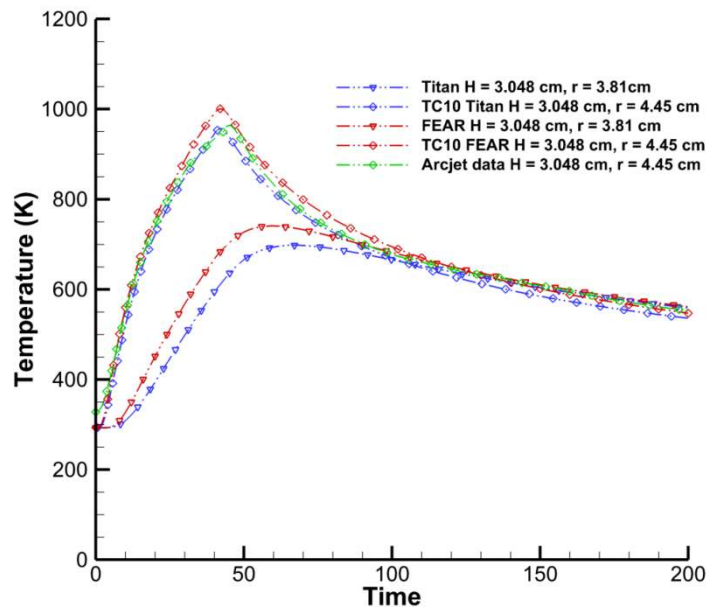

Fig. 8 Temperature comparison between FEAR and TITAN along a radial line at a depth of 3.048 cm.

The physics being modeled within FEAR are nearly identical to that of FIAT and TITAN except for how the pyrolysis gas flow is treated. FEAR solves Darcy's Law to determine both the magnitude and direction of the pyrolysis gas flow and the internal pressure. As a consequence, FEAR depends on the porosity of the material, permeability and pyrolysis gas viscosity. The database for these three properties is severely lacking and some

American Institute of Aeronautics and Astronautics

assumptions which are described in Ref. 5, must be made to arrive at a solution. Essentially, FEAR is introducing additional uncertainties and the thermal response model needs to be adjusted to account for them. If given the opportunity to make adjustments to the thermal response model, FEAR could be made to match the data as well as TITAN. With this new analysis capability, it is imperative that porosity, through-the-thickness and in-plane permeability, and pyrolysis gas viscosity be measured. Also, a proper database must be developed to reduce the uncertainty in these properties and a response model specific to FEAR must be developed.

VII. Conclusion

A 2-D axisymmetric analysis of an arcjet coupon constructed of PICA with an LI-2200 insulator was performed with the thermal response code FEAR. The solution results from FEAR compared well to both arcjet data and to the 2-D TITAN solution results. The thermal response code FEAR also calculated the stagnation point recession to within 0.78 mm of the measured recession. The anisotropic property representation implemented within FEAR was shown to be correct. The thermal response model required by FEAR may need to be adjusted slightly from the response model developed for TITAN in order for the calculations to correlate more closely with arcjet test data.

Acknowledgments

References

[1] Anon., "Space Shuttle Program Thermodynamic Design Data Book," Rockwell International, Report SD73-SH-0226, Downey, CA, Jan. 1981.

[2] Scotti, S. J., (compiled by), "Current Technology for Thermal Protection Systems", NASA-CP-3157, February 1992.

[3] Kratsch, K. M., Loomis, W.C., Randles, P.W., "Jupiter Probe Heatshield Design", AIAA 1977-427, AIAA/ASME 18th Structures, Structural Dynamics & Materials Conference, 21-23 March 1977.

[4] Balter-Peterson, A., Nichols, F., Mifsud, B. and Wendell, L., "Arc Jet Testing in NASA Ames Research Center Thermophysics Facilities", AIAA 1992-5041, 4th International Aerospace Planes Conference, 1-4 December 1992, Orlando, FL.

[5] Dec, J. A., "Three-Dimensional Finite Element Ablative Thermal Response Analysis Applied to Heatshield Penetration Design," Ph.D. Dissertation, Aerospace Engineering Dept., Georgia Institute of Technology, Atlanta, GA, 2010.

[6] Dec, J. A., "Multi-Dimensional Finite Element Ablation and Thermal Response Analysis", 43rd AIAA Thermophysics Conference, (submitted for publication), New Orleans, LA, 25-28 June 2012.

[7] Tran, H., Johnson, C. E., Rasky, D. J., Hui, F. C., Hsu, M.-T., Chen, T., Chen, Y.-K., Paragas, D., and Kobayashi, L., "Phenolic Impregnated Carbon Ablators (PICA) as Thermal Protection Systems for Discovery Missions," NASA TM-110440, April 1997.

[8] Covington, M. A., Heinemann, J. M., Goldstein, H. E., Chen, Y.-K., Terrazas-Salinas, I., Balboni, J. A., Olejniczak, J., and Martinez, E. R., "Performance of a Low Density Ablative Heat Shield Material," Journal of Spacecraft and Rockets, Vol. 45, No. 2, March–April 2008, pp. 237–247.

[9] Chen, Y.-K., Milos, F. S., "Two-Dimensional Implicit Thermal Response and Ablation Program for Charring Materials", *Journal of Spacecraft and Rockets,* Vol. 38, No. 4, Jul-Aug 2001, pp 473-481.

[10] Milos, F.S., and Chen, Y.-K., "Two-Dimensional Ablation, Thermal Response, and Sizing Program for Pyrolyzing Ablators", *Journal of Spacecraft and Rockets,* Vol. 46, No. 6, Nov-Dec 2009, pp. 1089-1099.

[11] Goldstein, H. E., "Kinetics of Nylon and Phenolic Pyrolysis", Lockheed Missiles and Space Company, Sunnyvale, CA. LMSC-667876, October 1965.

[12] Goldstein, H. E., "Pyrolysis Kinetics of Nylon 6-6, Phenolic Resin, and Their Composites", Marcel Dekker, Inc., New York, 1971.

[13] Huebner, K. H., Dewhirst, D. L., Smith, D. E., Byrom, T. G., The Finite Element Method for Engineers, 4th Ed., John Wiley & Sons, New York, 2001.

[14] Reddy, J. N., Gartling, D. K., The Finite Element Method in Heat Transfer and Fluid Dynamics, 3rd Ed., CRC Press, Boca Raton, pp. 175-176, 2010.

[15] Timoshenko, S. P., Goodier, J. N., Theory of Elasticity, 3rd Ed., McGraw-Hill, Inc., Chapter 1-2, 1987.

[16] Agrawal, P., Ellerby, D. T., Switzer, M. R., Squire, T. H., "Multidimensional Testing of Thermal Protection Materials in the Arcjet Test Facility", AIAA 2010-4664, 10th AIAA/ASME Joint Thermophysics and Heat Transfer Conference, 28 June – 1 July 2010, Chicago, IL.

[17] Marschall, J. and Milos, F. S., "Gas Permeability of Rigid Fibrous Refractory Insulators", AIAA-1997-2479, 32nd AIAA Thermophysics Conference, Atlanta, GA, June 23-25, 1997.